Zero-Touch-Design Information-Centric Wireless Sensor Networking with Availablity Assurance

Shintaro Mori
Department of Electronics Engineering and Computer Science
Fukuoka University
8-19-1 Nanakuma, Jonan-ku, Fukuoka 814-0180, Japan
e-mail: smori@fukuoka-u.ac.jp

***Abstract*—This paper presents a novel zero-touch-design information-centric wireless sensor network for smart-city applications. To promote self-growing in an autonomous-distributed environment, the proposed scheme adopts zero-touch technology implemented using micro-operators and micro-service providers with a focus on the lower layers where sensor nodes join the network. The scheme also aims to improve the overall availability by utilizing proxy caching and fragmented data management schemes. Computer simulations revealed that, for large-size sensing data (e.g., rich sensing data), the proposed scheme performs better when used with millimeter-wavelength band wireless networks. The results also showed that the scheme is effective in terms of availability and energy consumption. This study is a part of our ongoing research on the development of an ecosystem that enables a smart-city-as-a-service platform, where we are currently focused on the development and experimental trials through on-site testing.**

Keywords: Information-centric wireless sensor networks; Zero-touch-design; Availablity assuarance; Smart-city-as-a-service platform

I. INTRODUCTION

The Internet of things (IoT) has stimulated new trends and empowered innovative new developments in smart devices. The deployment of such devices at distributed locations is a typical scenario in smart-city applications. Wireless sensor networks (WSNs) are an elemental technology in this regard, and they require rapid deployment, initial configuration, and sensing-data provisioning, all of which remain challenging. Moreover, in next-generation wireless networks, such as beyond the fifth generation (5G), massive IoT devices will be deployed in a heterogeneous environment across multiple network domains and versatile service slices. Therefore, for scalability and sustainability, the IoT platform must be shifted from a centralized cloud-based framework to an autonomous-decentralized edge-based one that allows access from various end-users and applications ranging from individuals to enterprises or governments [2].

In light of this background, we focus on two key technologies: zero-touch and data-centric. The zero-touch design aims to completely automate the network management process to minimize the initial costs and set up individual execution environments. Ever since a zero-touch-design system was utilized in the first Linux operating system, there have been increased demands for service deployments that are versatile and flexible in cloud-native micro-services. As for the data-centric architecture, information-centric networking (ICN) (e.g., a content-centric network or named-data network) can be utilized to transform the current network world (e.g., the Internet). ICN natively supports functionalities, such as abstraction, naming, and in-network caching, which enables the data to be decoupled from its original location and the security of every piece of data to be adopted in the network layer. Combining ICN with WSNs is suitable for an autonomous-decentralized environment, which yields Information-Centric Wireless Sensor Networking (ICWSN) [3].

In our previous study [4], we investigated an ICWSN-based ecosystem with a blockchain for smart-city applications utilizing a scheme that achieves efficient and reliable caching. We also presented a blueprint for the system design of a zero-touch-design ICWSN on which the actual smart-city application services will be deployed [1]. In the current paper, utilizing these prior studies as a basis, we evolve and expand the ICWSN system with a focus on reliability and availability. We interpret reliability here as a benchmark indicating that the system operates correctly throughout a certain time interval, i.e., that a reliable system can tolerate any error that may occur (fault tolerant). We interpret availability as an indicator that a system is operating correctly and can continue running its functions at any time, i.e., a system with high availability should have undetectable periods of inaccessibility. In the proposed scheme, for reliability, we utilize a micro-operator (μO), where a network node can be joined only after the μO verifies its individual information when it turns on.

For system deployment in actual smart cities, to reduce the effort required for initialization, the first step is to enable automatic participation by the ICWSN. To this end, for zero-touch design, the proposed scheme also uses a micro-service provider (μSP). For the management of device information and application-service types in μOs and μSPs, the proposed scheme utilizes blockchain-based ledgers, as both the ICWSN and blockchain can work together under an autonomous-decentralized network without mutual trust. However, in ICWSNs, the network nodes are typically limited to resources and thus cannot feasibly support the blockchain network. The μOs provide a solution in that the proposed scheme guarantees the trustworthiness of the nodes during an initial process.

Therefore, the data generated by a reliable node can be trusted without needing to receive any additional verification. For this reason, blockchain-based storage for the data no longer requires traditional computation-intensive mining, and the blockchain can simply select alternative consensus schemes, (e.g., proof-of-authority or proof-of-elapsed-time algorithms) instead of the traditional ones [5]. For availability improvement, the proposed scheme utilizes proxy caching and cooperative data management schemes, where the proxy caching scheme transfers the role of responding to the sensing data from relatively low-reliability nodes to more reliable ones, and the cooperative data management is applied among the nodes that assigned the task of the proxy caching scheme.

In the proposed scheme, the protocol stacks are placed on the ICN layer of the wireless local area network (WLAN). Another option would be to directly place them on the datalink and physical layers, but this is not general purpose since it requires the construction of a special protocol suite. In addition, to support rich 3D sensing applications, virtual reality, augmented reality, and mixed reality, etc., in a future innovative society, the WLAN underpinning the proposed scheme should select the mesh network based on two radio-frequency bands, microwave and millimeter-wave (mmWave,) which are respectively specified as IEEE 802.11 ac/ax and IEEE 802.11 ad/ay. In our evaluation and feasibility demonstration of the proposed scheme, we focus on these two radio bands while performing system modeling, computer simulation, testbed development, and a fundamental experiment.

Section II of this paper presents an overview of the traditional technologies related to our work, and Section III describes the proposed scheme. In Section IV, we report the numerical results, and in Section V, we present the experimental results using a hardware-based testbed device. Related works are discussed in Section VI. We conclude in Section VII with a brief summary and mention of future work.

II. Wideband Information-Centric Wireless Networking Technologies

Various wireless communications and network systems have been investigated to meet different requirements regarding sensing-data collection, distribution, security, and privacy. This section presents an overview of ICWSNs and mmWave WLANs for wideband wireless communications.

A. Information-centric wireless sensor network

The ICWSN system deals with individual data as named data. For named data, one of two naming rules can be selected, hierarchical or flat, depending on the situation in which the ICWSN is deployed. When the data are wirelessly forwarded, the network nodes along the routing path cache (copy and store) them in the local storage for further retrieval of the same data. The caching method is generally categorized into on-path caching or off-path caching. On-path caching is an in-network caching scheme in typical ICNs, whereas in off-path caching, the nodes around the routing path also actively cache. Wireless communications are typically provided in a flooding (broadcasting) style, unlike wired networks, and this specific characteristic (i.e., overhearing phenomena) is what enables the off-path caching to be implemented. Thanks to these caching methods, the sensing data can be effectively expanded, making the retrieval accelerative.

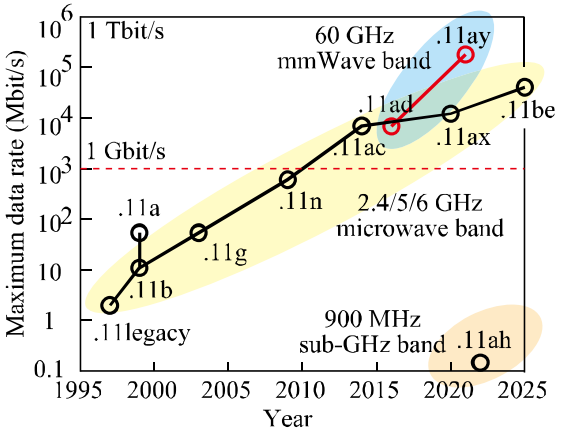

Figure 1. Evolution and history of wireless local area network in IEEE 802.11 specifications.

In the ICN layer, data packets are mainly transferred as interest and response packets. When data retrieval is performed, the requester sends the target packet to interest the network as an acquisition of the data. The node that receives the interest packet and matches the target data for this request plays the role of responder. The responder replies with the response packet encapsulated by the data. Note that, since the data is not distinguished from either the original or the cached data, the interest packet consists of data-requestor information and the properties of the required data. In contrast, the response packet includes the named data with a digital signature and lifetime (data freshness). For data exchange, the interest packets are forwarded to send back the data, and the trace information is recorded in the forwarding information base (FIB), which stores the outgoing interface(s) for each known naming prefix. The intermediate network nodes each have a pending interest table (PIT) that keeps a record of the incoming interfaces and the interest-packet information. The response packet follows the reverse path guided by the PIT entries, and these traversal records are removed while forwarding the data.

B. Wireless communications in mmWave band

The steadily increasing global demand for higher bandwidth has motivated the exploration of the underutilized mmWave spectrum. As shown in Figure 1, this spectrum has a higher potential than the microwave band (e.g., the sub-6-GHz and sub-GHz bands) and can be made available for much larger bandwidth allocation to enable the use of beamforming for greater spatial reuse. Historically, the mmWave has been utilized for fixed wireless access, but standards defined as IEEE 802.11 ad/ay have been commonly provided in the 60-GHz band [6] as well. Radio propagation in the mmWave band is characterized as free-space path loss and precipitation attenuation, which are typically a few dB per kilometer, unless heavy rain causes a significant attenuation (15 dB/km in

150 mm/hr). The 60-GHz band has further attenuation due to oxygen and the water concentration of objects, i.e., the 57–64 GHz bands are high-oxygen absorbing bands with 10–15 dB/km, and the moisture it contains (e.g., from leaves and humans) results in particularly strong attenuation across the radio path.

IEEE 802.11 ad is a member of the IEEE 802.11 family and the pioneer in standardizing the 60-GHz band (i.e., in the unlicensed 57–66 GHz bands). IEEE 802.11 ay is the latest standard for expanding the data-transmission rate up to 30 Gbit/s. The 60-GHz band has a greater amount of available bandwidth than all other unlicensed bands (e.g., 2.4, 5, and 6 GHz), but rain and atmosphere make the radio links useless; thus, it is currently utilized only for short-range indoor environments. This should be reconsidered because today's cellular-base-station cell size in urban areas is on the order of 200 m, which offers greater flexibility in the deployment of outdoor scenarios. Terragraph (TG) is an IEEE 802.11 ad/ay-compliant platform developed by Meta (Facebook) and has been successfully deployed by mobile operators and Internet service providers for the backhaul in wireless mesh networks [7].

The physical layer of mmWave WLAN uses a phased-array antenna to execute beamforming between the transmitter and receiver side nodes since the mmWave propagation results in severe path loss and signal attenuation. Note that beamforming technology can concentrate the transmission power and the receiver region over narrow beams. The medium access control (MAC) layer has similar functionalities to the traditional microwave band; however, TG's design only supports the single carrier PHY mode and 12 types of modulation and coding scheme (MCS) sets with data rates up to 4.6 Gbit/s.

III. Proposed Scheme

We introduce a receiver-side cooperation design into the ICWSN system to improve availability. The proposed scheme features two key technologies: proxy caching and fragmented data management. After modeling the ICWSN system, we describe the proposed scheme on the basis of the model.

A. Network model

The network structure of the proposed scheme consists of three main network sections: an ICWSN, an edge network, and a cloud network, as shown in Figure 2. The ICWSN includes sensor nodes (SNs) and relay nodes (RNs) as network nodes that are centrally orchestrated by a mobile base station (MBS). The SNs can perform a pull operation to answer the inquiries of other network nodes. Note that, in traditional WSNs, the sensing data is gathered for the cloud servers (push operation), and users retrieve it as needed. The SNs and RNs are both distributed across the smart-city area, and the SNs sense physical values. The sensing data are provided to users and then partially aggregated to the cloud network via the RNs and MBS. The RNs forward the data (as well as the legacy WSNs), and the data are cached in the local storage of the RNs (as well as the typical ICNs) during the data-forwarding process. The MBS is connected to both the ICWSN and the edge network, so it is relatively more resourceful than the SNs

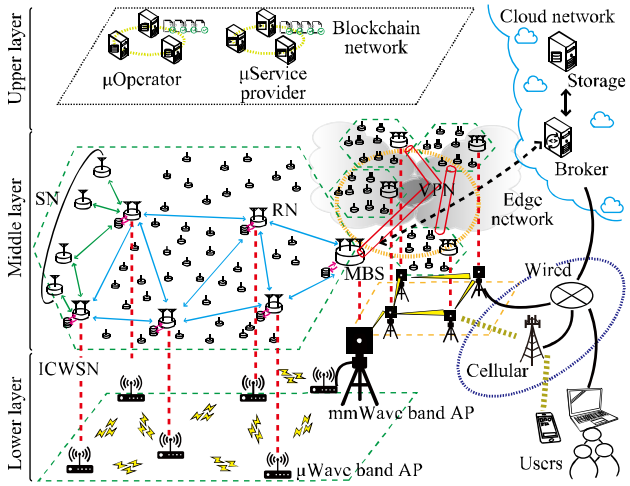

Figure 2. Overview of proposed scheme.

and RNs. The cloud network includes a storage server and a broker. The broker intermediates between the ICWSNs, edge networks, cloud networks, and users, i.e., it exchanges and translates the sensing data and the control messages between them as a gateway. This functionality enables interoperability between multiple regional ICWSNs and provides global scalability. The storage server stores and provides the (copied) partial caching data. Finally, the users are those who consume and obtain the data.

The proposed scheme utilizes two service providers to overlay the physical network for reliability and a zero-touch design: a micro-operator (μO) and a micro-service provider (μSP). The μO verifies whether the SNs can join the ICWSN and provides them with the required connectivity. The information provided here comprises either the authentication that an SN is a proper member of the ICWSN or the network construction settings for wireless transmissions. The former information is provided by the μO, and the latter is managed using the FIB in the RNs, MBS, and broker. The μSP provides the application service and its setting information for the registered SNs to perform as a specified actuator in the ICWSN. Namely, when an SN device is turned on, it sends a registration request to the μO and establishes a secure Virtual Private Network (VPN) link if approved. An ICWSN with a VPN implements the orchestration of distant ICWSNs, terminal fixation at the datalink layer, and secure data exchanges. After joining the network, the SN downloads and installs a configuration setting and application software from the μSP. (The detailed procedures regarding the initialization and registration are described in later sections.) In the proposed scheme, the databases to be referenced by μO and μSP should be used as distributed databases, such as a blockchain. This design principle ensures scalability across interregional networks with different governments, operators, and providers, which is effective in the smart-city scenario assumed in this paper.

As shown in Figure 2, as a network architecture, the proposed scheme uses a mesh network with IEEE 802.11 WLANs in the microwave and mmWave bands in the lower

layer. Since the ICWSN is constructed using WLANs, the ICWSN and edge network are in a closed local area network; meanwhile, we assume these networks can access the Internet via the wired or cellular network for global connection. The SNs, RNs, and MBSs can be virtually placed on the physical network in the middle layer, but they should also be placed on the WLAN access points for practical reasons related to location, power supply, and wireless features. The µOs and µSPs are deployed in the upper layer as a functionality of the overlay network technology.

B. Proxy caching scheme

One of the problems with ICWSNs is that SNs can suddenly disappear due to a lack of energy supply or the failure of a (cheap) device, and their turnover (including participating and withdrawing) is rapid because of node mobility. We overcome this problem by utilizing a proxy caching scheme, which ensures availability even in this situation.

An ICWSN consists of an MBS, several RNs, and several SNs, which can be expressed as a set of $\{\mathcal{R}, \mathcal{S}\}$. The set of RNs and SNs are respectively represented as $\mathcal{R} \triangleq \{r_0, r_1, r_2, \cdots, r_{|\mathcal{R}|}\}$ and $\mathcal{S} \triangleq \{s_1, s_2, \cdots, s_{|\mathcal{S}|}\}$. Note that r_0 is the MBS and the others are RNs, and the operator $|\mathcal{X}|$ is the number of elements in the set of $\mathcal{X}$. In the proxy caching scheme, the RNs around an SN are assigned as the SN's alternative nodes, named Proxy RNs (PRNs). The set of PRNs $\hat{\mathcal{R}}^{s_i}$ assigned to $\forall s_i$ $(\in \mathcal{S}, i = 1,2,\cdots,|\mathcal{S}|)$ is given by

$$\hat{\mathcal{R}}^{s_i} \triangleq \Omega(\mathcal{R}|s_i) = \{\hat{r}_1^{si}, \hat{r}_2^{si}, \cdots, \hat{r}_{|\hat{\mathcal{R}}^{s_i}|}^{si}\}, \quad (1)$$

where $\Omega(\mathcal{R}|s)$ is a function that lists up the set of RNs in which the members of $\mathcal{R}$ can be connected to s. In addition, we assume that the SN does not belong to multiple ICWSNs, i.e., there is no roaming across multiple µOs. In proxy-caching-enabled data retrieval, if s_i does not respond to the data-query request for any reason, one of the $\hat{\mathcal{R}}^{s_i}$ answers instead of s_i. The privilege of each $\hat{\mathcal{R}}^{s_i}$ is prioritized in accordance with its index, from small to large; specifically, $\hat{r}_1^{si}$ is called the primary PRN. The priority among $\hat{\mathcal{R}}^{x_i}$ is determined based on the wireless channel condition when the SN is initially registered to the ICWSN or should be re-registered when it moves.

C. Data fragmentation and its cooperative management

For the data fragmentation and management scheme, let $X^{s_i,t}$ denote the data generated by s_i at time t. The expired data, $X^{s_i,t+t_0}$, no longer has any value, where t_0 is the period of valid data. If the data size is large, it is divided into smaller chunks. Let $\delta^{s_i t}$ denote the number of fragmentations for $X^{s_i,t}$; then, this method can be expressed as

$$X^{s_i,t} = x_1^{s_i,t} \oplus x_2^{s_i,t} \oplus \cdots \oplus x_{\delta^{s_i,t}}^{s_i,t}, \quad (2)$$

where the operator $\oplus$ is a bit-by-bit combining. The PRNs cooperatively deal with the divided data and not only perform data backup but also reduce the cost of unnecessary stockholding when the data becomes worthless.

When not all data is complete during alternative data retrieval, the primary PRN gathers the partial loss of chunks from the other PRNs and compiles them. Among PRNs, the primary PRN is most likely to store the divided data, and the amount of available data will be limited in accordance with the size of its index. In some cases, however, only a certain chunk may be lost, which can be dealt with by using the scheme of erasure code and cooperative communications [8]. Using this technique, even if not all the data is complete (i.e., if some of them are lacking), the original data can be fully restored based on the incomplete divided data.

D. Procedure of proposed scheme

In this section, we present the signal processing procedure of the proposed scheme. When a new SN is appended to the ICWSN, it must be identified and its information recorded on the member nodes of the ICWSN. As shown in Figure 3(a), the SN sends a registration request to the neighbor RNs, and the message is then forwarded between RNs and delivered to the µO via the MBS. Note that the SN selects a primary PRN from among the available PRNs here. The µO inquires and verifies the SN's identification to the blockchain network. If the SN is officially approved and activated, the µO sends back the message of complete registration. In this process, the MBS registers the SN as a member of the ICWSN, and the PRNs know that it is the SN to which they should provide a proxy caching mechanism. In addition, it is properly updated in the FIB of the MBS and the RNs on the traced-back routing path. After the SN has been registered, it requests a pre-defined execution (actuation) from the µSP and downloads the application (and its configuration) to enable a zero-touch initialization. Note that a kind of image file is downloaded data for the virtual operating system (e.g., Docker).

When the SN moves, it takes over the task of the proxy caching scheme for the new PRNs, which includes selecting and registering them. As shown in Figure 3(b), the SN sends a withdrawal request to the current PRNs, but the primary PRN temporarily keeps this request on hold, and the SN simultaneously sends a reconstruction request to the neighboring RNs in a new location. A new primary PRN is selected and broadcasts the decision to the ICWSN. On the basis of this notification, the old primary PRN accepts the withdrawal request and removes its task from the old PRNs. In addition, the new and old PRNs should update their FIB at the same time. Through this process, the set of PRNs is changed from $\hat{\mathcal{R}}^{s_i}$ to $\hat{\mathcal{R}}^{s'i}$ corresponding to the movement from s_i to s_i', which is given by

$$\hat{\mathcal{R}}^{s_i'} \triangleq \Omega(\mathcal{R}|s_i'). \quad (3)$$

The PRNs of $\{\hat{\mathcal{R}}^{s_i} \cup \hat{\mathcal{R}}^{s_i'} - \hat{\mathcal{R}}^{s_i'}\}$ remove the registered s_i, and the RNs of $\{\hat{\mathcal{R}}^{s_i'} - \hat{\mathcal{R}}^{s_i} \cap \hat{\mathcal{R}}^{s_i'}\}$ newly register it. If the user moves to a different ICWSN, it is necessary to obtain the wireless-connection information from the µO and re-install and reconfigure the application service from the µSP.

If the radio channel is temporarily degraded (e.g., in the case of not receiving the data continuously), it is expected to recover over time, but since the reason typically originates from a failure of the SN device (e.g., a lack of battery supply,

continuous busy status, or permanent poor radio condition), the RNs should detect the cause and reassign the PRNs accordingly. As shown in Figure 3(c), the primary PRN initiates and sends the diagnosis message to the other PRNs. If the PRNs without a primary PRN have also not received the data, the result is reported to the μO, and then the appropriate action is conducted, such as notifying the manager to repair the SN device. When one of the PRNs has received the data, i.e., the primary PRN's radio channel is permanently worse, the secondary PRN takes over the primary PRN's task: specifically, the primary PRN sends the change of primary assignment message to the secondary PRN to switch their duties. If the secondary PRN suffers from a similar situation, it can be replaced by the third PRN, thus maintaining an optimal primary PRN selection.

If the data-requestor cannot directly access the ICWSN, (e.g., if a user cannot access the ICWSN via the Internet), the interest packet is alternatively sent from the broker. Note that users are not limited to human users, they also include the machine that periodically retrieves the collected data. As shown in Figure 3(d), if the required data have been cached in the cloud network, MBS, or RNs close to the MBS, the responder node replies with the cached data; otherwise, the primary PRN answers.

E. Formulation of proposed scheme's availability

In this section, we formulate the effect of the proposed scheme in terms of availability. When introducing system reliability engineering to the network research field, we can define availability as the probability of a data-retrieval request being successfully answered. The availability of the system can be calculated based on the summation of the network node's availability and the outage probability of wireless networks. The network node's availability A is calculated based on

$$A = T_{\mathrm{MTBF}} / (T_{\mathrm{MTBF}} + T_{\mathrm{MTTR}}), \quad (4)$$

where T_{MTBF} is the mean time between failures and T_{MTTR} is the mean time to repair. As for the outage probability of the wireless link, p_{o}, it is determined based on the radio-frequency band and radio-propagation environment, which will be modeled and illustrated in the next section.

Let A_{SN}, A_{RN}, and A_{MBS} denote the availability of SN, RN, and MBS, respectively. The RNs located close to the MBS have a greater effect on the availability of the overall system due to not only hardware failure but also network traffic (and its congestion). To simplify our analysis here, we ignore this effect, i.e., we assume the average availability, $\bar{A}_{\mathrm{RN}}$, for all RNs. For the same reason, we use the average outage probability, $\bar{p}_{\mathrm{o}}$, instead of p_{o} for time-varying channel conditions. Let A_{conv} and A_{prop} denote the availability of the overall conventional scheme and the proposed scheme, respectively, which can be calculated based on

$$A_{\mathrm{conv}} = (1-\bar{p}_{\mathrm{o}}) A_{\mathrm{SN}} \cdot A_{\mathrm{MBS}} \cdot \prod_{n=1}^{N_{si}} (1-\bar{p}_{\mathrm{o}})\, \bar{A}_{\mathrm{RN}} \quad (5)$$

and

$$A_{\mathrm{prop}} = A_{\mathrm{PRN}}^{s_i} \cdot A_{\mathrm{MBS}} \cdot \prod_{n=1}^{N_{s_i}-1} (1-\bar{p}_{\mathrm{o}})\, \bar{A}_{\mathrm{RN}}, \quad (6)$$

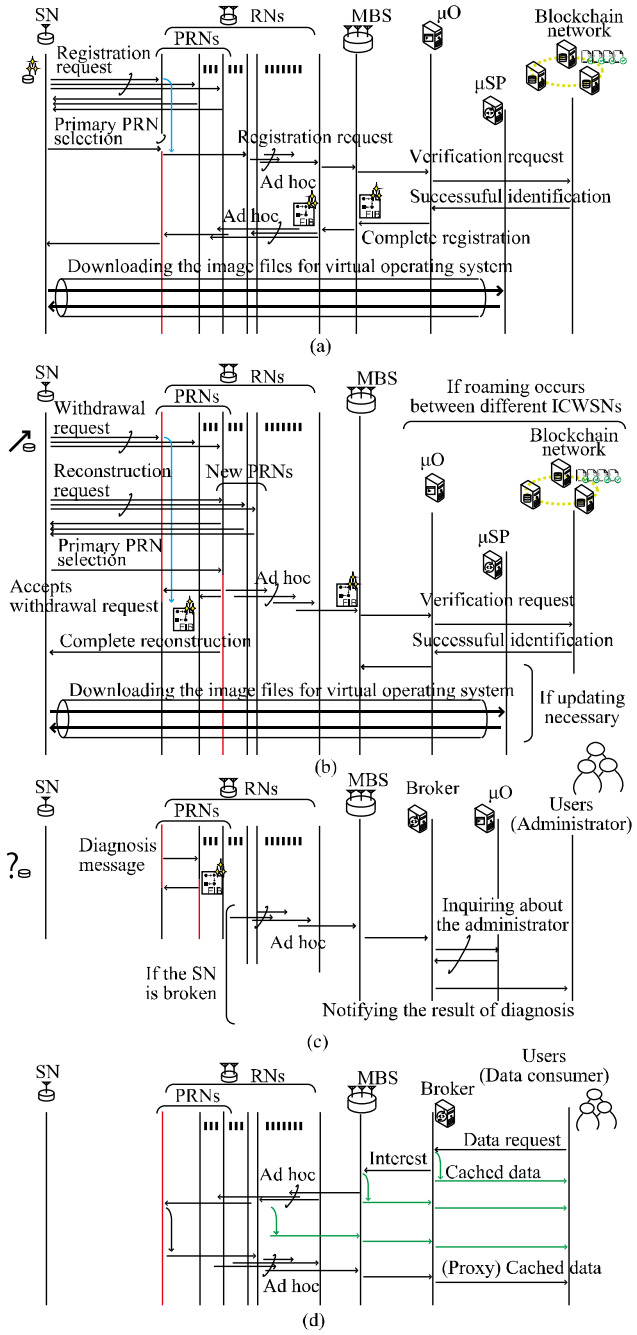

Figure 3. Procedure of the proposed scheme: (a) an SN is newly appended to the ICWSN, (b) the SN moves and changes its PRNs, (c) the SN's data does not reach the PRNs, and (d) the data is retrieved for the ICWSN from the users (data consumers).

where N_{s_i} is the number of hops from the primary PRN of s_i to the MBS, and $A_{\mathrm{PRN}}^{s_i}$ is the availability of the PRNs for s_i, which is given by

$$A_{\mathrm{PRN}}^{s_i} \triangleq 1 - [\, 1 - (1-\bar{p}_{\mathrm{o}}) \bar{A}_{\mathrm{RN}} \,]^{|\hat{s}[s_i]|}. \quad (7)$$

By comparing (5) and (6), the availability section of the SN in the first term is replaced by a parallel RN, which leads to an availability improvement thanks to the proxy caching. This is because, the relationship between them is $A_{\mathrm{RN}} > A_{\mathrm{SN}}$, since the SNs are generally cheap and massively spread around in the observation area. At the same time, we need to ensure that A_{MBS} has a smaller failure rate, since the MBS is the single point of failure in a physical ICWSN and the proposed mechanism cannot change this. We adopt a high-reliability (industrial use) hardware device as a testbed demonstration in order to mitigate this issue, as discussed in the later section. It should therefore have the highest availability compared to all other nodes, i.e., $A_{\mathrm{MBS}} \gg A_{\mathrm{RN}} > A_{\mathrm{SN}}$.

F. Modeling of wireless communications

Radio propagation in the microwave and mmWave bands is typically characterized as free-space path loss. This can generally be represented as

$$L^{\propto d} = 20\log_{10}(\lambda/4\pi d_0) + 20\log_{10}(d/d_0) \ + \chi_{\mathrm{s}}\ (\mathrm{dB}), \quad (8)$$

where λ (= $300/f_{\mathrm{c}}$ MHz) is the wavelength of the carrier frequency f_{c}, d is the distance between the transmitter- and receiver-side nodes, and d_0 is the closed-in free-space reference distance (typically set to 100 m). χ_{s} is a shadowing variation, i.e., it is a random variable with a Gaussian distribution. Using the practical-experiment-based radio propagation model, (8) can be rewritten as

$$L^{\propto d} = \alpha + \beta \cdot 10\log(d) + \chi_{\mathrm{s}}\ (\mathrm{dB}), \quad (9)$$

where α and β are decided based on the individual radio propagation model. For example, we select the model of Erceg et al. [9] for the link between the nodes on the ground and the model of Amorim et al. [10] for the link between the ground- and air-nodes, as these models are formulated based on the experimental measurements for their respective practical scenarios. Specifically, in Erceg's model, in particular, β can be given by

$$\beta = (a - bh + c/h) + \varepsilon \cdot z, \quad (10)$$

where h denotes the antenna height, z is a random variable with the Gaussian distribution of $\mathcal{N}(0,1)$, and a, b, c, and ε are constant values depending on the surrounding environment [9]. In Amorim's model, α and β are constantly given depending on the UAV altitude [10].

In the microwave band, the link budget, i.e., the relationship between the transmission power P_{TX} and received signal strength $P_{\mathrm{RX}}^{\mathrm{microwave}}$, is represented by

$$P_{\mathrm{RX}}^{\mathrm{microwave}} = P_{\mathrm{TX}} - L^{\propto d} + G_{\mathrm{ANT}} - L_{\mathrm{DEV}}\ (\mathrm{dB}), \quad (11)$$

where G_{ANT} and L_{DEV} are the antenna gain and device loss, on both the transmitter- and receiver-side nodes. In contrast, the radio propagation in the mmWave band is characterized as not only free-space path loss but also precipitation attenuation, which is typically a few decibels per kilometer, unless heavy rain. The moisture is influenced by the presence of natural materials (e.g., leaves, humans), which results in particularly strong attenuation across the radio path. Therefore, the received signal strength in the mmWave is given by

$$P_{\mathrm{RX}}^{\mathrm{mmWave}} = P_{\mathrm{TX}} - L^{\propto d} + G_{\mathrm{ANT}} - L_{\mathrm{DEV}} - L_{\mathrm{RAIN}} - L_{\mathrm{O}^2} - L_{\mathrm{H_2O}}\ (\mathrm{dB}) \quad (12)$$

where L_{RAIN}, L_{O^2}, and $L_{\mathrm{H_2O}}$ are atmosphere attenuation due to rain, oxygen, and natural moisture materials, respectively.

The statistical distribution of the outage probability under the condition that P_{RX} exceeds the desired signal power $P_{\min}$ can thus be given by

$$p_{\mathrm{o}} = \Pr\left(P_{RX} > P_{\min}\right) = 1 - Q\left(\frac{P_{\mathrm{RX}} - L^{\propto d}}{S_{\sigma^2}}\right), \quad (13)$$

where $Q(x)$ is the Gaussian Q function defined as

$$Q(y) \triangleq \int_{\xi}^{\infty} \frac{1}{\sqrt{2\pi}} \mathrm{e}^{-\frac{\xi^2}{2}} \mathrm{d}\xi\,. \quad (14)$$

When p_{o} is simply obtained from the received power, (13) suffices; otherwise, in practice, the signal-to-noise ratio (SNR) should be considered in accordance with the modulation method and additive noise. In this case, (13) is rewritten as

$$p_{\mathrm{o}} = \Pr(\gamma_s < \gamma_0) = \int_0^{\gamma_0} \frac{1}{\gamma_s} e^{-\gamma/\gamma_s} \mathrm{d}\gamma, \quad (15)$$

where γ_s is the received SNR and γ_0 is the required SNR.

IV. Computer Simulation

In this section, we conduct computer simulations to clarify the conditions under which the proposed system can perform, identify numerical examples of availability, and evaluate its power consumption for deployment in a smart city.

A. Simulation environment

The computer simulations were implemented in C++ language on a PC (Windows 10 OS, Core i5 2.9 GHz, 16 GB RAM). Assuming an experimental network composed of 1,000 SNs, ten RNs, and an MBS, we implemented a scenario in which all SNs send the sensing data to the MBS via the PRNs. In the simulation, these nodes are deployed in a 1-km^2 area. The communication range of the nodes is equal in distance and all of them have the same outage probability.

B. Conditions under which the proposed system performs

Let ℓ denote the distance between the SN and RN and ρ denote the number of randomly distributed RNs per km^2. Figure 4 shows the relationship between the number of SNs that do not have PRNs in the case where ρ = 50, 100, 150, 200, and 250. As ℓ increases, the percentage of SNs with no PRNs decreases because the RNs that come under the coverage of the SN increase. Here, ℓ should be kept as small as possible because increasing it would require additional energy consumption for wireless communications. Note that, according to Shannon's information theory, the communication capacity is linearly increased based on the radio bandwidth and logarithmically increased based on the

SNR, and thus more energy consumption is necessary to expand the communication distance of ℓ. In addition, for larger ρ, the area assigned to the RNs as the PRNs becomes smaller, and thus the percentage also decreases. Since a larger ρ requires the placement of more RNs with higher functionalities (i.e., more expensive hardware equipment) compared to SN, ρ should be reduced from the viewpoint of cost reduction. Consequently, we set ℓ = 200 m, 150 m, 120 m, 100 m, and 80 m for ρ = 50, 100, 150, 200, and 250, respectively, as the minimum communication distance under no SNs without having PRNs. The computer simulation results will be evaluated on the basis of these parameters.

For data retrievals, Figure 5 shows the probability of successful data acquisition for the average outage probability of the wireless link $\bar{p}_o$. Figure 5(a) shows the case where the ICWSN responds to the proposed method of PRN cooperation, while (b) shows the case where only PPRN responds. As we can see, the curves in the cases of different ρ overlap and the evaluation results do not differ, which indicates that the data retrievals are not affected if a sufficient ℓ is assured and determined for ρ. Therefore, the proposed scheme is available (scalable) if appropriate parameters are given for the network scale for the pair of ρ and ℓ that makes up the parameters determined depending on the observation-area environment. As shown in Figure 5(a), the proposed scheme can reduce the response failures to 5% or less under $\bar{p}_o < 0.4$: specifically, the probability of data-retrieval success is 0.986, 0.978, 0.974, and 0.966 in the case where $\bar{p}_o$ = 0.1, 0.2, 0.3, and 0.4, respectively. From this result and the comparison of Figures 5(a) and (b), it is clear that the proposed scheme can improve the probability of data-retrieval success by 9.87%, 23.79%, 39.22%, and 60.65% in the case where $\bar{p}_o$ = 0.1, 0.2, 0.3, and 0.4, respectively, thanks to a PRN cooperation. However, in the case where $\bar{p}_o > 0.5$, i.e., under the poor wireless channel condition, the curves experience rapid degradation, making it difficult to improve the data-retrieval success even if the proposed scheme is introduced.

Figure 6 shows the mean number of PRNs with which the PPRN requests cooperation to collect data for PRNs. Specifically, this result represents the number of PRNs required to cooperate with each other until all the data divisions are completed. In Figure 6(a), the number of fragmentations is set to 10, while in (b), thanks to the erasure code, we assume that the original data can be recovered if ten of the 15 divided data are complete. With increasing $\bar{p}_o$, more cooperative PRNs are necessary because fewer divided data are cached in the RNs. When we compare Figures 6(a) and (b), it is clear that the use of the erasure code reduces the number of PRNs for data retrieval. This is an advantage when it comes to data acquisition, even though the total amount of sensing data increases during data generation. Specifically, the method with the erasure code improves by 53.7%, 55.2%, 53.3%, and 51.9% when $\bar{p}_o$ = 0.1, 0.2, 0.3, and 0.4, respectively. In particular, as shown in Figure 6(b), in the case where $\bar{p}_o < 0.05$, the number of cooperative PRNs is reduced to 0, which means that the data request can be fully completed by PPRN.

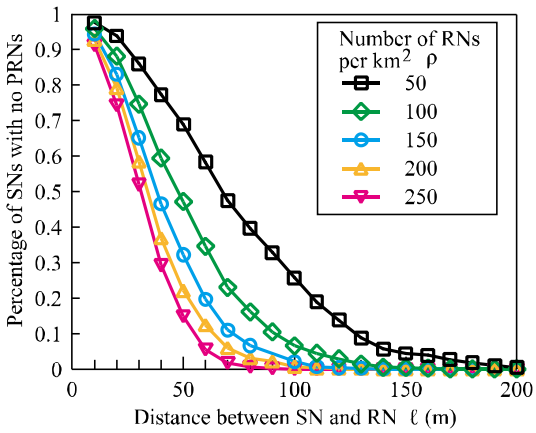

Figure 4. Percentage of SNs with no PRNs vs. distance between SN and RN.

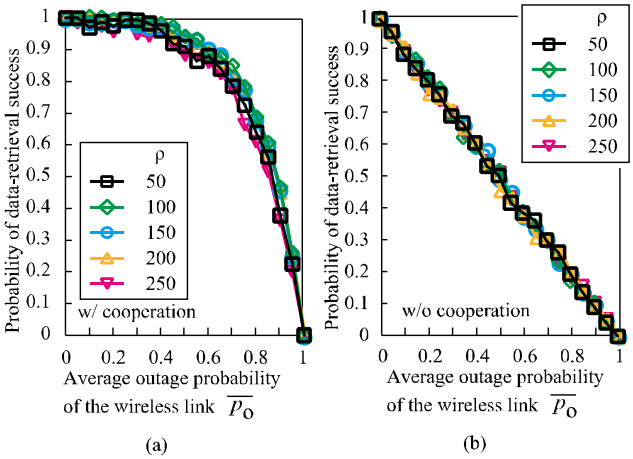

Figure 5. Probability of data-retrieval success vs. average outage probability of the wireless link under (a) proposed PRN cooperative environment and (b) conventional no cooperation PPRN-only environment.

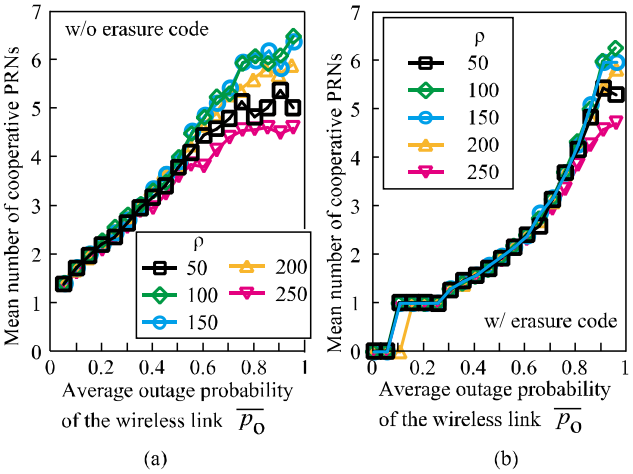

Figure 6. Mean number of cooperative PRNs vs. average outage probablity of the wireless link (a) without erasure code and (b) with erasure code.

C. Evaluation results: Availability

In this section, we calculate the availability modeled in the previous section using computer simulations. Figure 7 shows a numerical example in the case where ρ = 50 (ℓ = 200) and ρ = 250 (ℓ = 80). These simulations were performed under three conditions where (a) SNs were more unreliable than RNs and MBS, (b) MBS and RNs were equally reliable, and (c) MBS was more reliable than SNs and RNs. Note that, as shown in (6), the overall availability can be improved in the proposed scheme thanks to the proxy caching scheme, i.e., the system uses reliable PRNs instead of unreliable SNs. As a comparable method, the conventional scheme was not used the proxy caching technique. In addition, the MBS is a single point of failure in the ICWSN system.

The results are shown in Figures 7(a–c), where we can see that the proposed scheme improves the overall availability by 5.93%, 14.7%, 22.1%, 31.8%, 36.6%, and 46.7% for ρ = 50 (ℓ = 200) and 5.91%, 14.5%, 23.3%, 31.2%, 38.8%, and 46.0% for ρ = 250 (ℓ = 80) in the case where $\bar{p}_o$ = 0, 0.05, 0.1, 0.15, 0.2, and 0.25, respectively. As shown in Figure 7(a), SN devices were inferior to those of RNs (i.e., A_{RN} = 0.99 and A_{MBS} = 0.999, which was the same condition, but A_{SN} was 0.95 versus 0.9). In terms of overall (ICWSN system) availability, the conventional scheme had a difference (with the cases under that A_{SN} was 0.95 versus 0.9) of 5.56%, while the proposed scheme experienced no degradation.

Figure 7(b) shows the results when the availability of the RN and MBS is in the same condition, with a difference of 0.91% for both the proposed and conventional schemes. This result, which can be explained by the relatively unreliable MBS driving the overall availability, indicates that the proposed scheme cannot ensure the overall availability of the MBS with low reliability. However, as shown in Figure 7(c), in the case where the MBS is more reliable (i.e., A_{MBS} = 0.9999 and 0.99999), the overall availability was only improved by 0.09% and 0.1% compared to the case of A_{MBS} = 0.9999. Therefore, the results in Figure 7(b) suggest that the MBS should be more reliable than RNs and SNs, but the results in (c) indicate that the overall availability does not significantly improve even if the MBS device is over-reliable due to paying much cost, such as high-reliable hardware-device development.

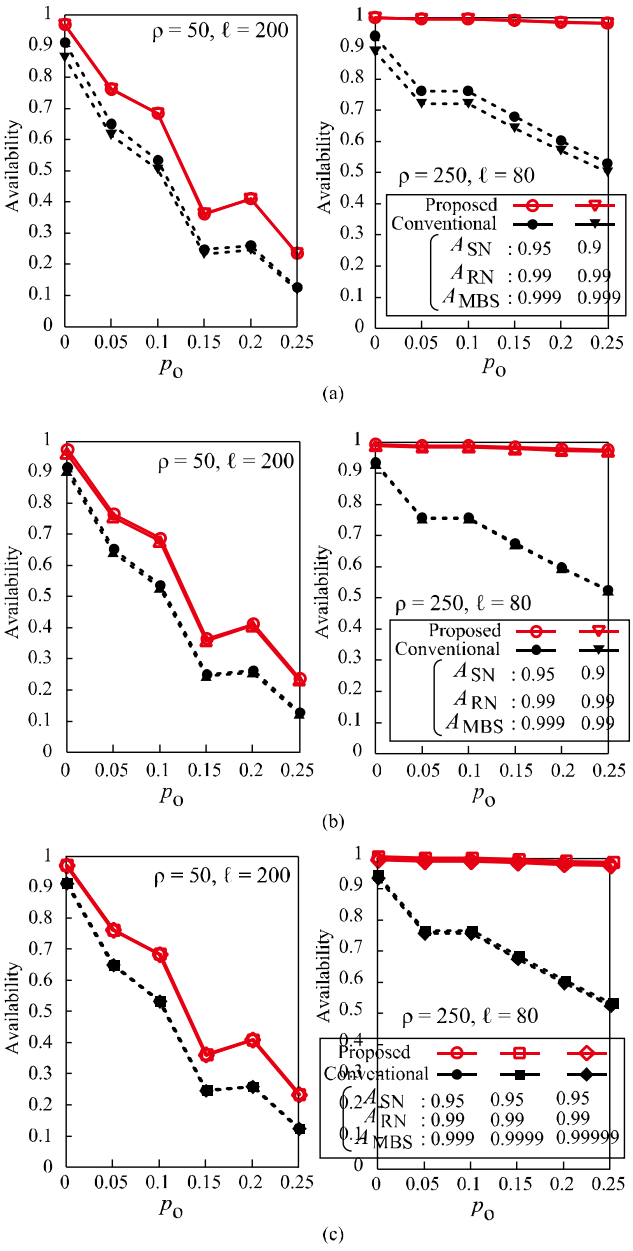

Figure 7. Computer simulation results for availability under three condintions: (a) SNs are unreliable, (b) MBS and RNs are equally reliable, and (c) MBS is more reliable than other nodes.

D. Evaluation results: Energy consumption

The challenge in deploying the proposed scheme is how to ensure a benefit in terms of energy consumption among the SN devices. This is because ICN has a pull-type network design and must always be on standby, and the blockchain also causes energy wastage. Figure 8 shows the computer simulation we ran to investigate the cumulative energy consumption in the conventional scheme (current application-programming-interface-based IoT platform) and the proposed scheme. Note that, when the SN does not execute any process, we assume the conventional scheme supports a sleep state with deep sleep and wake-up functionalities, whereas the proposed scheme waits in the idle state to be ready for data retrieval from any other node (because of the pull-type data acquisition). The energy consumption for each status is based on the actual measured values from our previous study [5].

As shown in Figure 8(a), the proposed scheme can reduce energy consumption by 1.91% if there are no additional requests for data retrieval in most cases of periodic data collection in ordinary situations. Moreover, even if 66 additional data retrievals per day are requested, the proposed scheme can outperform. Next, Figure 8(b) shows the total energy consumption in the ICWSN for 1,000 SNs, with the results converted into the power consumption per node. For these results, the number of data retrieval attempts for each

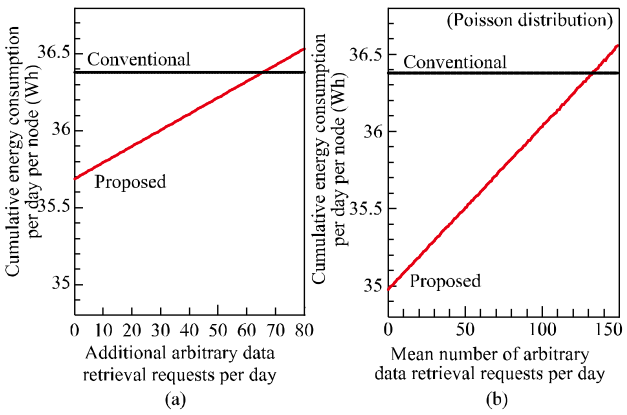

Figure 8. Simulation results for (a) additional data retrieval requests per day vs. cumulative energy consumption and (b) mean number of additional requests according to a Poisson distribution vs. cumulative energy consumption per unit for 1,000 SNs.

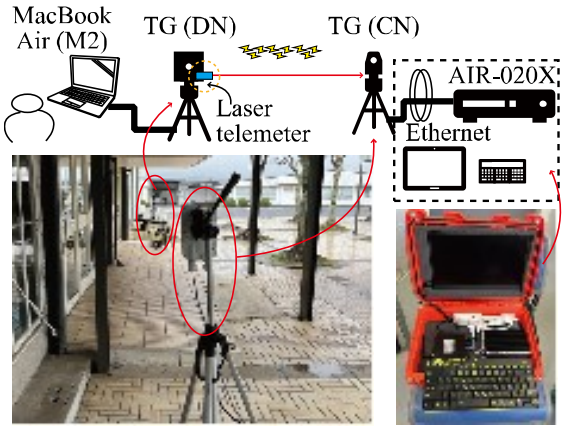

Figure 9. Experiment network and testbed device

TABLE I SPECIFICATIONS OF TG NODES

Spec.	MLTG-DN		MLTG-CN
Size	20×20×20 cm		18×11×4.3 cm
Weight	3.9 kg		1.1 kg
Frequency	f_c = 58.32 GHz (57.0–59.4 GHz)		
Tx power	43 dBm		38 dBm
Antenna	Gain: 28 dBi		Gain: 22 dBi
	Phased array antenna with 64 elements Azimuth range: -45° to +45° Elevation range: -25° to +25°		
LAN	Gigabit Ethernet (1x port)		
MCS no.	Modulation	Rate	Throughput
#9	π/2-QPSK	13/16	2,503 Mbit/s
#12	π/2-16QAM	3/4	4,620 Mbit/s

node was determined by a Poisson distribution, which is a more realistic calculation than the one in Figure 8(a). As we can see, the proposed scheme was able to reduce energy consumption by 3.85% and was advantageous until 138 retrieval attempts.

V. EXPERIMENTAL RESULTS

In this section, we implemented a testbed device and conducted a preliminary evaluation of the network performance, particularly for mmWave band WLANs. Note that we omitted the microwave band WLAN here because it is widely used and its features are well-known. The testbed here demonstrates a part of sensing-data processing and wireless communications for SN, RN, or PRN. Namely, the device will be able to perform the baseline tests for future test field construction and sensor node implementations. The testbed was implemented using an Advantech [11] AIR-020X (Six-core ARM v8.2 CPU, 8-GB RAM, Ubuntu 18.04 with Jet Pack OS), which is embedded in equipment for industrial use and adheres to the form factor of the NVIDIA Jetson; thus, the software and settings can be easily moved from any other prototype platform. The AIR-020X is high-performance for rich 3D sensing data, and we integrated it here with peripheral devices into a rectangular attaché case as a portable unit, as shown in Figure 9. The portable testbed device includes an IoT router, which is used to connect to the Internet via the cellular network for external time synchronization and emergency external control. The electrical power can be supplied from a wall outlet, through the devices can also alternatively be provided from the internal power-supply hub as well as the USB type A and C connections.

For the mmWave distribution networks, we utilized a pair of TGs consisting of distribution nodes (DNs) and client nodes (CNs), the specifications of which are listed in Table I. The TG was designed to construct a wireless mesh network. In particular, the DNs work and provide a backhaul wireless network, while the CNs can provide broadband wireless communications to the end users. In this paper, we evaluate the fundamental characteristics of mmWave communications, i.e., the link between the DN at the end of the backhaul network and the CN to the user terminal. Note that the hardware equipment for demonstrating the link between CN and DN and between DNs is different wireless communication equipment. However, we believe there is no significant difference in wireless communication characteristics.

According to the TG specification [9], a DN provides a mesh network among DNs within 15 hops and is composed of multiple sectors capable of communication in different directions. A CN is typically a one-sector station node that terminates Internet protocol (IP) connectivity for an end-user. The communication protocol between a DN and CN corresponds to the model of access point to station node in IEEE 802.11 ad/ay. To determine the best beam angle for the best SNR, TG has features of periodic beamforming and interference measurement. The MCS set is a combination of a modulation method (specifically BPSK, QPSK, or 16-QAM) and the low-density parity check coding scheme (with code rates of 1/2, 5/8, 3/4, 13/16, and 7/8). TG supports a total of 12 MCSs and typically operates at MCS nos. #12 and #9 (as

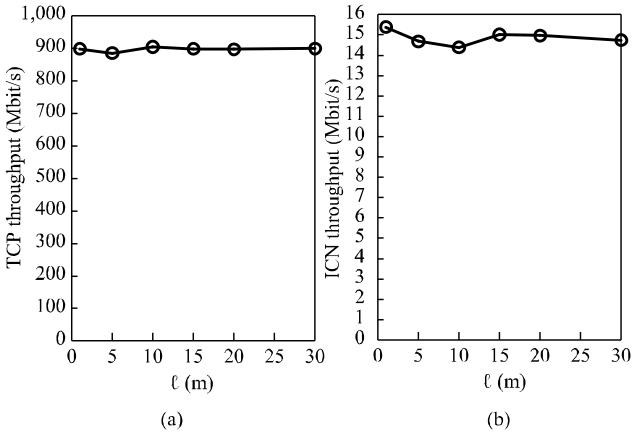

Figure 10. Experimental results for (a) TCP throughput and (b) ICN throughput vs. distance between SN and RN in mmWave WLAN.

shown in Table I) for 250-m-range coverage and achieves a throughput of 1 Gbit/s.

In the experiment, the network nodes are constructed using the implemented portable device and a 13-in MacBook Air. The TG equipment was mounted on a tripod, and both were respectively connected to the subscriber- and publisher-side devices. The horizontal plane of a DN and CN was maintained using a laser telemeter and the distance between the two nodes was measured at the same time.

This experiment was conducted in an outdoor environment, as shown in Figure 9, and there were no objects to interrupt the radio route, although some of the surrounding buildings caused reflections. The radio propagation was dominated by line-of-sight and building-reflected paths. Figure 10 shows the experimental results, including throughput at the transmission control protocol (TCP) layer using iPerf3, a common tool for measuring TCP throughput, and the ICN layer using Cefore [12], a CCNx-based ICN platform. Note that, when the proxy caching scheme is used, there might be a problem of cache inconsistency. In Cefore, the caching data can be managed using database in the daemon process of csmgrd and this concern is not present. As we can see, there was no significant throughput degradation depending on the distance between TGs, unlike that seen with IEEE 802.11 standards in Sub-6-GHz bands. In this experiment, we remove the reasons for the degradation of radio propagation, e.g., radio attenuation by trees and foliage, blocking materials (vehicle and human) between antennas, and multipath fading due to reflected waves. In addition, the mmWave communication must have the beamforming technique to bolster strong straightness with w signal weakness. In fact, the throughput was reduced by up to 50% when a person crosses between nodes, and throughput was reduced by up to 10% when the horizontal plane was not flat.

Since the mmWave band is highly directional (i.e., it has a radio-propagation characteristic similar to that of light), we investigated the degree to which it can be tolerated once a communication path between antennas was established by a beamforming technique. The DN and CN were placed three meters apart from each other, and we conducted the

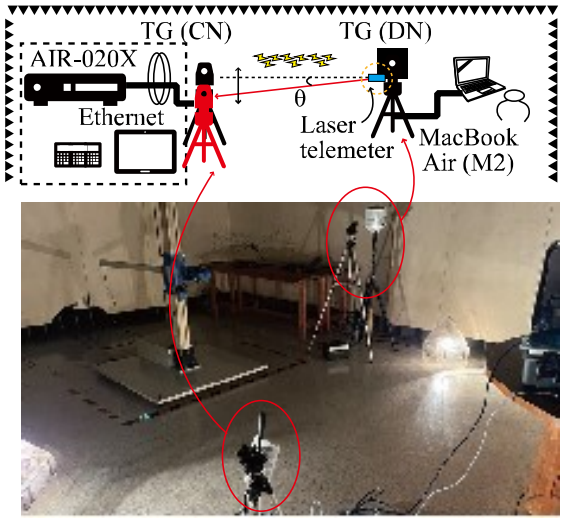

Figure 11. Overview of experimental site in anechoic chamber (shielded room).

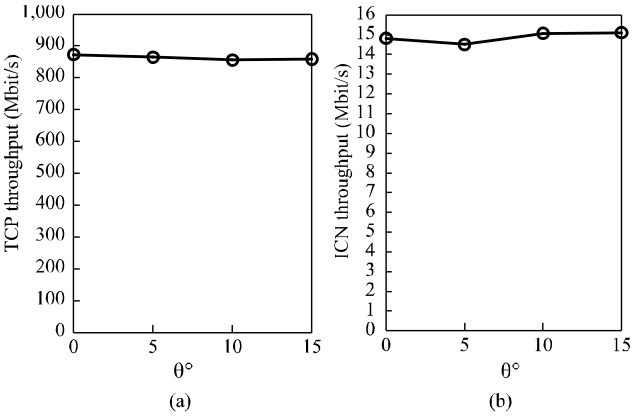

Figure 12. Experimental results for beamforming technique: (a) TCP throughput and (b) ICN throughput vs. degree from the horizontal plane in mmWave WLAN.

experiment in an electromagnetic anechoic chamber that is a shielded to eliminate the effect of other radio signals, including the reflected waves themselves. The DN and CN were maintained on a horizontal axis (determined using a laser telemeter), and the TCP and ICN throughputs were measured when the DN was fixed and the CN was moved to change its angle, as shown in Figure 12. The results showed that the wireless communication was stable and maintained even if the angle between CN and DN was changed several times. Note that, in our latest study [13], we develop and evaluate the testbed devices and test fields to evaluate the effectiveness of the proposed scheme for real WSN implementations.

VI. Related Work

Zero-touch management has become a hot topic in the process for standardization, e.g., by the European Telecommunications Standards Institute (ETSI) Zero-Touch Network and Service Management (ZSM) working group. Sanchez-Navarro et al. [14] provided a novel holographic immersive network management interface that extends the

standardized ETSI ZSM reference architecture to enable network administrators to understand real-time automated tasks in a 5G network without human intervention. Boškov et al. [15] proposed a zero-touch solution based on WLAN and Bluetooth technologies that can yield a sufficient performance for provisioning multiple devices without depending on the vendor's proprietary hardware and software. For resource management among nodes including an extended capability regarding 5G network slicing services, Theodorou et al. [16] formed marketplaces to facilitate the exchange service level agreements, where a blockchain was utilized for guaranteeing an untrusted and unreliable node.

For μO and μSP, Togou et al. [17] introduced a distributed blockchain-enabled network slicing framework that enables service and resource providers to dynamically lease resources, thereby ensuring high performances for their end-to-end services. The key component of the framework is its global service provisioning, which provides admission control for incoming service requests along with dynamic resource assignment by means of a blockchain-based bidding system. This is essentially a blockchain-based multi-operator service provisioning for 5G users with Intra and Inter spectrum management among multiple telecom operators. Gorla et al. [18] presented a blockchain-based implementation model for spectrum sharing between operators to minimize spectrum under-utilization in order to enable reliable quality of services. Another study [19] has suggested that the network slice provider will play the role of an intermediate entity between the vertical service provider and the resource provider, which makes a shift from a network-operator-oriented business to a more open system with multiple actors. Today, management and orchestration are considered prime components of the new network management layer [20], and multi-domain orchestration has helped in simplifying infrastructural operations while enabling better scaling and faster deployment of network services. Based on multi-constraint QoS, it fulfills the E2E slice request. Blockchain is also deployed to ensure trustworthiness between different telecom operators, introduce transparency, and automate the fulfillment of service-level agreements through smart contracts.

For mmWave-band communication systems, Rappaport, et al. [21] presented path loss models with directional and omnidirectional antennas based on over 15,000 measured power delay profiles (PDPs) at 28, 38, 60, and 73 GHz bands using wideband channel sounders. Tariq, et al. [22] measured received signal strength and delay spread values for each specified beam combination with massive antenna arrays in both indoor and outdoor scenarios using TG radios. Shkel, et al. [23] presented TG platform for promoting the research in mmWave propagation, systems, and networks. Aslam, et al. [24] measured the radio propagation characteristics for in-street backhaul environments and evaluated along with lay-based simulations. The results indicated that path loss in the urban canyon scenario was observed to be smaller when compared with the residential areas due to the rich number of multipath components. All these studies indicate that mmWave features a high path loss and a high material attenuation.

Sellami, et al. [25] proposed to implement an architecture for a distributed fog caching solution for ICN system, which consisted of sensor sub-networks connected to one or more fog super-nodes that maintained the internal caching policies and interactions with the fog in order to achieve efficient content caching and retrieval. Sukjaimuk, et al. [26] proposed an effective caching and forwarding algorithm for congestion control for ICWSN. The scheme utilized accumulative popularity-based delay transmission time for forwarding strategy and included the consecutive chunks-based segment caching scheme. Zhang, et al. [27] leveraged the machine learning technology to propose an intelligent caching scheme that could automatically adjust the caching nodes' caching parameters for the dynamic network environments. The simulation results showed that the scheme outperformed the existing approaches in terms of the total energy consumption.

VII. Conclusion

In this paper, we presented a zero-touch-design ICWSN to promote self-growing and ensure a reliable sensing-data distribution in which multiple players actively participate and exchange data. A computer simulation was conducted using a testbed of the proposed scheme and TG to investigate the conditions under which it can best perform, its overall availability, and its energy consumption, as the potential waste involved in the use of ICN and blockchain is significant. The results demonstrated the feasibility of our scheme and clarified the radio-propagation characteristics of mmWave band WLANs. In our ongoing research project, which we call the Decentralized Digital Twins' Ecosystem (D2EcoSys), we will further investigate the deployment of this scheme for real smart cities, which is our future work.

Acknowledgment

This work was partly supported by NICT Japan, Grant Number 05601. We are grateful to Dr. Kenji Kanai for his helpful discussions, and Advantech Japan, BeMap, Haft, Panasonic, and TEAD for their help with the on-site experiments.

References

[1] S. Mori, "A study on zero-touch-design information-centric wireless sensor networks," *Proc. IARIA the 22th Int. Conf. Networks (ICN 2023)*, Apr. 2023, pp. 7–9.

[2] H. Chergui, A. Ksentini, L. Blanco, and C. Verikoukis, "Toward zero-touch management and orchestration of massive deployment of network slices in 6G," *IEEE Wireless Commun.*, vol. 29, no. 1, pp. 86–93, Feb. 2022.

[3] B. -S. Kim, C. Zhang, S. Mastorakis, M. K. Afzal, and J. Tapolcai, "Guest editorial special issue on information-centric wireless sensor networking (ICWSN) for IoT," *IEEE Internet of Things J.*, vol. 9, no. 2, pp. 844–845, Jan. 2022.

[4] S. Mori, "Information-centric wireless sensor networks for smart-city-as-a service: Concept proposal, testbed development, and fundamental evaluation," *Proc. IEEE Consumer Commun. and Networking Conf. (CCNC 2023)*, Jan. 2023, pp. 945–946, doi: 10.1109/CCNC51644.2023.10060577.

[5] S. Mori, "Secure caching scheme using blockchain for unmanned aerial vehicle-assisted information-centric wireless sensor networks," *J. Signal Process.*, vol. 26, no. 1, pp. 21–31, Jan. 2022.

[6] Y. Ghasempour, C. R. C. M. Silva, C. Cordeiro, and E. W. Knightly, "IEEE 802.11ay: Next-generation 60 GHz communication for 100 Gb/s Wi-Fi," *IEEE Commun. Mag.*, vol. 55, no. 12, pp. 186–192, Oct. 2017.

[7] A. Nordrum, "Facebook pushes networking tech: The company's Terragraph technology will soon be available in commercial gear," *IEEE Spectrum*, vol. 56, no. 4, pp. 8–9, Mar. 2019.

[8] S. Mori, "Data collection scheme using erasure code and cooperative communication for deployment of smart cities in information-centric wireless sensor networks," *Int. J. Advances in Networks and Services*, vol. 14, no. 3&4, pp. 54–64, Dec. 2021.

[9] V. Erceg et al., "An empirically based path loss model for wireless channels in suburban environment," *IEEE J. Sel. Areas in Commun.*, vol. 17, no. 7, pp. 1205–1211, July 1999.

[10] R. Amorim et al., "Radio channel modeling for UAV communication over cellular networks," *IEEE Wireless Commun. Lett.*, vol. 6, no. 4, pp. 514–517, Aug. 2017.

[11] Advantech, https://advantech.com/ (retrieved: Nov. 2023).

[12] Cefore, https://cefore.net/ (retrieved: Nov. 2023).

[13] S. Mori, "Test-field development for ICWSNs and preliminary evaluation for mmWave-band wireless communications," *Proc. IEEE Consumer Commun. and Networking Conf. (CCNC 2024)*, Jan. 2024. (in press)

[14] I. Sanchez-Navarro, P. Salva-Garcia, Q. Wang, and J. M. A. Calero, "New immersive interface for zero-touch management in 5G networks," *Proc. 2020 IEEE 3rd 5G World Forum (5GWF)*, Sept. 2020, pp. 145–150, doi: 10.1109/5GWF49715.2020.9221116.

[15] I. Boškov, H. Yetgin, M. Vučnik, C. Fortuna, and M. Mohorčič, "Time-to-provision evaluation of IoT devices using automated zero-touch provisioning," *Proc. IEEE GLOBECOM 2020*, Dec. 2020, pp. 1–7, doi: 10.1109/GLOBECOM42002.2020.9348119.

[16] V. Theodorou et al., "Blockchain-based zero touch service assurance in cross-domain network slicing," *Proc. 2021 Joint European Conf. Networks and Commun. & 6G Summit (EuCNC/6G Summit)*, June 2021, pp. 395–400, doi: 10.1109/EuCNC/6GSummit51104.2021.9482602.

[17] M. A. Togou et al., "DBNS: A distributed blockchain-enabled network slicing framework for 5G networks," *IEEE Commun. Mag.*, vol. 58, no. 11, pp. 90–96, Nov. 2020.

[18] P. Gorla, V. Chamola, V. Hassija, and N. Ansari, "Blockchain based framework for modeling and evaluating 5G spectrum sharing," *IEEE Network*, vol. 35, no. 2, pp. 229–235, Mar.–Apr. 2021.

[19] B. Nour, A. Ksentini, N. Herbaut, P. A. Frangoudis, and H. Moungla, "A blockchain-based network slice broker for 5G services," *IEEE Networking Lett.*, vol. 1, no. 3, pp. 99–102, Sept. 2019.

[20] V. K. Rathi et al., "A blockchain-enabled multi domain edge computing orchestrator," *IEEE Internet of Things Mag.*, vol. 3, no. 2, pp. 30–36, June 2020.

[21] T. S. Rappaport, G. R. MacCartney, M. K. Samimi, and S. Sun, "Wideband millimeter-wave propagation measurements and channel models for future wireless communication system design," *IEEE Trans. Commun.*, vol. 63, no. 9, pp. 3029–3056, Sept. 2015.

[22] M. H. Tariq, I. Chondroulis, P. Skartsilas, N. Babu, and C. B. Papadias, "mmWave massive MIMO channel measurements for fixed wireless and smart city applications," *Proc. IEEE 31st Annual Int. Sympo. Personal, Indoor, and Mobile Radio Commun. (PIMRC 2020)*, Sept. 2020, pp. 1–6, doi: 10.1109/PIMRC48278.2020.9217375.

[23] A. Shkel, A. Mehrabani, and J. Kusuma, "A configurable 60GHz phased array platform for multi-link mmWave channel characterization," *Proc. IEEE Int. Conf. Commun. (ICC 2021)*, June 2021, pp. 1–6, doi: 10.1109/ICCWorkshops50388.2021.9473724.

[24] M. Z. Aslam, Y. Corre, J. Belschner, G. S. Arockiaraj, and M. Jäger, "Analysis of 60-GHz in-street backhaul channel measurements and LiDAR ray-based simulations," *Proc. 14th European Conf. Antennas and Propagation (EuCAP)*, Mar. 2020, pp. 1–5, doi: 10.23919/EuCAP48036.2020.9135946.

[25] Y. Sellami, G. Jaber, and A. Lounis, "Distributed fog-based caching solution for content-centric networking in IoT," *Proc. IEEE Consumer Commun. and Networking Conf. (CCNC 2022)*, Jan. 2022, pp. 493–494, doi: 10.1109/CCNC49033.2022.9700561.

[26] R. Sukjaimuk, Q. N. Nguyen, and T. Sato, "An efficient congestion control model utilizing IoT wireless sensors in information-centric networks," *Proc. Joint Int. Conf. Digital Arts, Media, and Technol. with ECTI Northern Sec. Conf. Electrical, Electronics, Comp. and Telecommun. Eng.*, Mar. 2021, pp. 210–213, doi: 10.1109/ECTIDAMTNCON51128.2021.9425753.

[27] Z. Zhang, X. Wei, C. -H. Lung, and Y. Zhao, "iCache: An intelligent caching scheme for dynamic network environments in ICN-Based IoT networks," *IEEE Internet of Things J.*, vol. 10, no. 2, pp. 1787–1799, Jan 2023.